Atomic Insights into the Structural Properties and Displacement Cascades in Ytterbium Titanate Pyrochlore (Yb2Ti2O7) and High Entropy Pyrochlores

M. Mustafa Azeem * and Qingyu Wang

Posted Date: 18 August 2023

doi: 10.20944/preprints202308.1329.v1

Keywords: Molecular dynamics simulation, ytterbium pyrochlore oxides, nuclear waste substrate, displacement cascades, lattice constants, high entropy alloys, LAMMPS

Article

Atomic Insights into the Structural Properties and Displacement Cascades in Ytterbium Titanate Pyrochlore ($Yb_2Ti_2O_7$) and High Entropy Pyrochlores

M. Mustafa Azeem [1]*, Qingyu Wang [2]

[1] Department of Civil, Architectural, and Environmental Engineering, Missouri University of Science and Technology, Rolla, MO 65409, USA; mustafa@mst.edu
[2] College of Nuclear Science and Technology, Harbin Engineering University, Harbin, 150001, China; ravian20052007@yahoo.com
* Correspondence: mustafa@mst.edu; Tel.: +1-205-535-6402

Abstract: Pyrochlore oxides ($A_2B_2O_7$) are potential nuclear waste substrate material due to their superior radiation resistance properties. We performed molecular dynamics simulations to study the structural properties and displacement cascades in ytterbium titanate pyrochlore ($Yb_2Ti_2O_7$). We computed threshold displacement energy (E_d) and lattice constant (a_o) of $Yb_2Ti_2O_7$. The effect of displacement cascades in $Yb_2Ti_2O_7$ of recoils of energies 1 keV, 2 keV, 5 keV, 10 keV in different crystallographic directions ([100], [110], [111]) were studied. The number of defects is found to be proportional to the energy of incident PKA. Additionally, the E_d of pyrochlore is computed and it exhibits anisotropy. Furthermore, radiation damage in high-entropy pyrochlore (HEPy) i.e., $YbYTiZrO_7$, $YbGdTiZrO_7$, $Yb_{0.5}Y_{0.5}Eu_{0.5}Gd_{0.5}TiZrO_7$ were investigated and compared with $Yb_2Ti_2O_7$. It was found that HEPy have a larger E_d as compared with $Yb_2Ti_2O_7$ which exhibits characteristic of lower radiation damage resistance than HEPy. Our simulation proposed that HEPy alloys are more radiation resistant than individual pyrochlore constituents . This work will provide atomic insights in developing substrate materials for nuclear waste applications.

Keywords: molecular dynamics simulation; ytterbium pyrochlore oxides; nuclear waste substrate; displacement cascades; lattice constants; high entropy alloys; LAMMPS

1. Introduction

Despite the environment-friendly and high-efficacy energy source nuclear energy has few distinctive concerns [1–3]. Commercial use of nuclear power is only evident when radioactive waste management is done under a proper strategy.[4]. Therefore, the reprocessing of spent fuel is an important part of ensuring nuclear safety and environmental safety. Nuclear wastes are in different forms depending on the sources and radioactive concentration [5]. Solidification of liquid waste is a common process for managing nuclear waste disposal. In this regard, the most common processes are vitrification and synroc methods [6]. Although borosilicate glass is being used frequently as nuclear waste substrate matrix but having low solubility of actinide elements restrict their usage [7]. An alternate substitute to solve this limitation are ceramics pyrochlore due to their superior durability, better potential at high temperatures and humid environments [8,9]. Moreover, ceramic has high values of waste loading as compared to glass [10]. The ceramic-based substrate with the minor addition of ionic concentration has higher radiation stability and excellent chemical and physical properties [11]. Long term radiation damage is critical for nuclear waste disposal strategy [12]. Pyrochlore has been developed rapidly as high-entropy ceramics waste substrate materials in recent years [13,14]. Future state of the art nuclear reactors involving the recycling of nuclear fuels and burning of minor actinide series and decontamination of fission fragments [15]. Titanate pyrochlore ($Yb_2Ti_2O_7$) has been demonstrated as an effective waste substrate material for pyrochemical reactions [16,17].

Minervini et al.; reported disorder in different pyrochlore oxides using the atomic scale simulation method [18]. Additionally, pyrochlore demonstrated stability range dependence on the

relative size of cations [19]. Brendan et al.; have investigated the relationship between the structural and bonding energy in lanthanide pyrochlore oxides (Sn_2O_7) and found that the position parameter of the oxygen vacancies is inversely proportional to the lattice parameter. Recently, Zhang et al, have reported the machine learning (ML) methods to determine lattice constants of different multi-substitutional pyrochlores in the range of 9-11 Å [20]. Moreover, the pyrochlore stannate ($Ce_2Sn_2O_7$) demonstrated temperature-dependent anisotropic nature [21]. Superconductivity of ternary pyrochlore oxide ($Cd_2Re_2O_7$) reported by Sakai et al., at 1.1K , and the lattice constant was found to be 10.22 Å at room temperature [22]. Liyuan et al.; performed molecular dynamics to study structural and elastic properties of different pyrochlores under numerous combinations of A and B cations. It was found that displacement energy in pyrochlores strongly depends on the energy of the incident PKA's as well as their atomic masses [23]. They also reported that lattice parameters and atomic radius predominantly affect structural as well as thermal properties. Chartier et al., performed molecular dynamics simulations to study displacement cascades in lanthanum zirconate pyrochlore ($Ln_2Zr_2O_7$) with uranium ions bombarded at 350 K with 6 keV along different orientations . It was observed model doesn't lose its crystallinity [24]. It is reported in earlier studies that displacement cascade is a determinant of material radiation stability [25]. Atomic scale radiation damage studies in pyrochlores ($Gd_2Zr_2O_7$) have demonstrated healing mechanism during radiation [12,26]. Moreover, a combination of different anion and cations result in a radiation-resistant response of pyrochlores [27]. Pyrochlores have disordered structures due to irradiation and alteration of thermodynamics [28]. Pyrochlores are known for their radiation-resistant properties, primarily because of their inherent structural stability.. This structure allows for the migration and annihilation of defects, minimizing their impact on the material's overall properties.

High entropy pyrochlores refer to a class of materials that exhibit high configurational entropy due to the random distribution of multiple cations on the crystal lattice sites. These materials have been studied for various applications, including radiation tolerance. High entropy pyrochlore (HEPy) oxides synthesized with $Yb_2Ti_2O_7$ are obtained by substituting the cations in pyrochlore structure and they have displayed higher radiation resistance than their individual pyrochlore [29–31]. Atomic scale simulation results have also displayed that radiation resistant are affected by addition of Zr content in HEPy [32,33].

Defects dynamics in pyrochlore type structures is quite difficult to determine in experimental studies due to complex structure and associate irradiation associated phenomena [23,34]. The displacement cascades involve the initiation of damage in the materials that alternately determine the long term possible outcomes. Atomic scale simulation methods can shed light on determining the fundamental material properties and interaction mechanisms in pyrochlores [35–44]. It is also important to mention that a limited number of experimental and simulation studies have been performed on the behavior of different pyrochlore under radiation [7,12,29,45–54]. Molecular dynamics simulations have been applied to study the influence of displacement cascades on the microstructural properties of different pyrochlores [7,12,20,48,49,54,55]. Computer simulations interpret the radiation damage as a predictive tool for processing the experiments. The simulation models describe the physics behind the phenomena responsible for radiation damage mechanism in irradiated material by providing valuable tools observed in nuclear power plants (NPP). Numerous radiation damage studies have been reported on metals and alloys [36,38–43,56–68]. This study will serve as a predictive model for providing insight into expected behavior in radioactive environments.

This article studies three aspects of pyrochlores oxides . Primarily, interatomic potential was established by parametrizing existing literature and later validated through calculation for equilibrium lattice, atomic radius threshold energy of different combination of A and B in pyrochlore structure and was performed. Furthermore, displacement damage cascades simulations of $Yb_2Ti_2O_7$ were performed with each constituent elements with corresponding E_{PKA}~1, 2, 5, 10 keV in different incident directions. Moreover, high entropy alloys have been constituted with compositional adjustment of rare earth elements. The relation of irradiation stability was evaluated to determine the nature of $Yb_2Ti_2O_7$ was compared with high entropy pyrochlores.

Preprints (www.preprints.org) | NOT PEER-REVIEWED | Posted: 18 August 2023 doi:10.20944/preprints202308.1329.v1

2. Computational Details and Methodology

2.1. Crystal Structure

Pyrochlore have cubic fluorite-type structures containing 5 or more elements with oxygen-deficient vacancies having $A_2B_2O_7$ type structure with A (rare-earth) and B (transition metal) being different cations [69,70]. The 'A' position coordinated with 3^+ cation while 'B' position coordinated with 4^+ cation atoms, e.g. 3^+ cation (La^{3+}, Nd^{3+}, Gd^{3+}, Sm^{3+}, Y^{3+}) and 4^+ cation (Zr^{4+}, Ti^{4+}, Mo^{+4}) [71]. Moreover, 1/8 of the oxygen atoms are vacant to balance the charge [5]. The different ion combinations are used to compute different structural properties. The crystal structure is developed by Visualization of Electronic and Structural Analysis (VESTA) [72]. The lattice parameter for pyrochlore oxide was set as 10.194 Å. The initial model comprised of 8 unit cells with 88 atoms per unit cell with $Fd\bar{3}m$ group having composition $Yb_{16}Ti_{16}O_{56}$. Periodic boundary conditions were applied along axes. The initial structure was equilibrated using steep decent method (SD) since this method is considered a quick approach for an optimal efficient solution [73].

Figure 1 displays the computational model and unit cell of pyrochlore, where (a) MD snapshot of a relaxed computational model under study and (b) a unit cell of generic representation of pyrochlore [74]. The characteristic crystal structure of pyrochlores consists of a network of corner-sharing tetrahedra, which provides an open framework that can accommodate defects induced by radiation damage [75,76]. Molecular dynamics simulations were performed by a large-scale atomic/molecular massively parallel simulator (LAMMPS) developed by Plimpton [77] and structure analysis and visualization was done by OVITO developed by ppt [78].

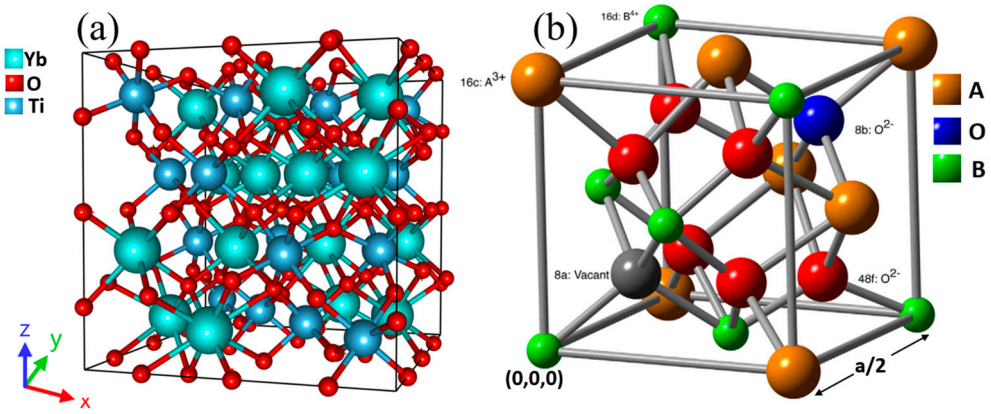

Figure 1. Schematic representation of computational model and unit cell of pyrochlore, (a) MD snapshot of a computational model $Yb_2Ti_2O_7$ (b) Unit cell of pyrochlore $A_2B_2O_7$ where A and B are transition metals [74].

2.2. Interatomic Potential

In MD simulation realistic interatomic potentials are very crucial for reliable results [79]. The interatomic potential was modified by coupling potential developed in earlier studies [18,80,81]. This potential was test for replicating equilibrium lattice constants and lattice constants reported in earlier studies. The potential function is divided into two parts and all pair interactions are described separately. The short-range -combination of ZBL (Ziegler-Biersack-Littmark) potential and Buckingham potential are adjoined with fitting function for smooth truncation. The long-range potential- coulomb potential, and the algorithm uses the particle-particle particle-mesh solver (PPPM) summation algorithm with an accuracy up to 10^{-4} and with r_{cutoff} =10 Å [82]. The Buckingham potential result in negative infinity due to short range whereas ZBL potential is more realistic for charged modes at short ranges interactions [83]. The piecewise interatomic potential of $Yb_2Ti_2O_7$ is expressed in Eq. (1), where $r_{1,2}$ is active range of potentials. The ZBL potential and Buckingham potential is fitted with fourth order exponential function ($V_{\text{Fit. fun}}(r_{ij}) = c_1 + c_2 r_{ij} + c_3 {r_{ij}}^2 + c_4 {r_{ij}}^3$) for smooth interconnection, where c_{1-4} are fitting constants.11111111

Preprints (www.preprints.org) | NOT PEER-REVIEWED | Posted: 18 August 2023 doi:10.20944/preprints202308.1329.v1

$$V(r_{ij}) = \begin{cases} V_{ZBL}\,(r_{ij}) & r_{ij} < r_1 \\ V_{Fit.\,fun}\,(r_{ij}) & r_1 < r_{ij} < r_2 \\ V_{Buck.}\,(r_{ij}) & r_2 < r_{ij} < r_{cut} \\ 0 & r_{cut} < r_{ij} \end{cases} \quad (1)$$

$V_{ZBL}=\frac{1}{4\pi\varepsilon_0}\frac{Z_1Z_2e^2}{r_{ij}}G(\alpha)$ where $G(\alpha)= 0.18118e^{-32\alpha}+0.5099e^{-0.9423\alpha}+0.2802e^{-0.4029\alpha}+0.02817e^{-0.2016\alpha}$ and $\alpha=\frac{r_{ij}(Z_1^{0.23}+Z_2^{0.23})}{0.8854a_0}$. The notation in above expression such as ε_0 represents dielectric constant a_0 is the Bohr's radius, e is the electronic charge and Z_1, Z_2 are atomic number of elements. The atomic numbers of Yb_{70} , O_8 and Ti_{48} . The potential function of Buckingham $V_{Buck.}\,(r_{ij})$ potential is represented as function of distance in Eq. 2, where A_{ij}, ρ and C_{xy} are element dependent potential parameters.

$$V_{Buck.}(r_{ij}) = A_{ij}\, e^{-\frac{r_{ij}}{p}} - \frac{C_{XY}}{r_{ij}^{6}} \quad (2)$$

The parameters for Buckingham potential as function interatomic distance for Yb and O satisfying condition in Eq. 1. The values of the parameters are set for each computed pairs in Table 1 reported by earlier studies [18,23]. For Ti-O, the value of C_{xy} is adjusted for smooth truncation. Before testing the potential further separately , interatomic potentials were coupled through splined function to ZBL repulsive and Buckingham functions . The resulting functions are plotted in Figure 2. The connected potentials for cation-anion/anion-anion are computed through Table 1 , while cation-cations are defined by pair style automatically computed by LAMMPS mentioned in the previous studies[84,85].

Table 1. Buckingham potential and splined function parameters [18,23].

Pair (s)	A_{ij}(eV)	ρ(Å)	C_{xy} (eVÅ^6)	c_1(eVÅ^{-1})	c_2(eVÅ^{-2})	c_3(eVÅ^{-3})	c_4(eVÅ^{-4})	r_1(Å)	r_2(Å)
Yb-O	1649.80	0.3386	16.57	10.40	-8.38	3.08	-0.55	0.6	1.3
Ti-O	2131.40	0.3038	0.400	10.62	-14.80	-14.74	-6.28	0.3	2.0
O-O	9547.96	0.2192	32.00	9.355	-10.71	6.23	-1.68	0.8	2.1

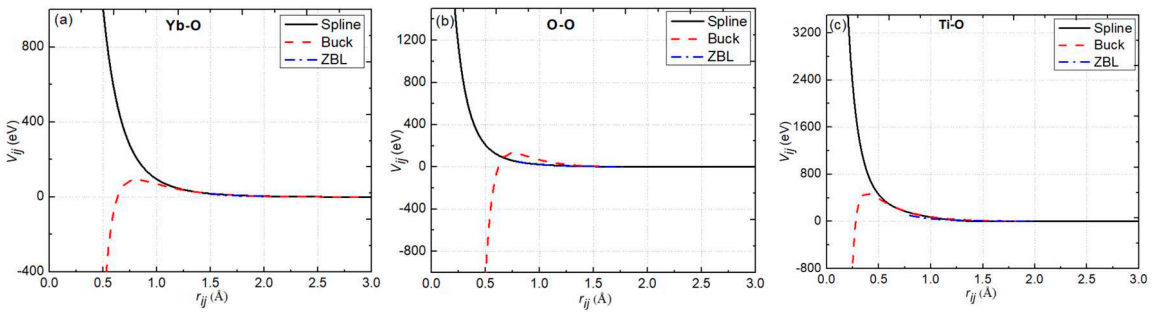

Figure 2. Potential as function of distance between pairs fitted by splined ZBL and Buckingham for (a) Yb-O, (b) O-O , (c) Ti-O.

2.3. Displacement Cascades Simulations

Displacement cascade simulations were performed through molecular dynamics code LAMMPS [86]. A system having dimension 10×10×10 with a total of 88000 were constructed . Our calculation for lattice parameters resulted in 10.09 Å with periodic boundary set along all axes. Interatomic potential function was employed as mentioned in previous section . After completing the preliminary settings, thermal relaxation was performed initially using canonical (NVT) ensemble at 300K with 0.001ps for a simulation time of 30ps. After the thermal relaxation, the model was relaxed again using

Preprints (www.preprints.org) | NOT PEER-REVIEWED | Posted: 18 August 2023 doi:10.20944/preprints202308.1329.v1

microcanonical ensemble (NVE) at a time step of 0.0001ps for another 10ps to ensure the system has attained sufficient equilibrium before proceeding displacement cascade simulation. For damage cascade simulations , the recoil energies were chosen as 1 keV, 2 keV, 5 keV and 10 keV. The direction of PKA's were set at 45° along xy plane at 7° to avoid channeling effects. The selected PKA were Yb atoms and PKA's angles are all included with the positive Z axis to prevent channeling effect.

3. Results and Discussion

3.1. Calculation for Equilibrium LATTIce Constant

The sites on A and B in structure have different ions and their combination affects the properties of the pyrochlores. An important parameter of the unit cell is the lattice constant and its equilibrium properties . Figure 3 displays total energy as function of lattice constant of $Yb_2Ti_2O_7$. The relation concave curve indicates that energy of the system will reach the minimum at a certain equilibrium lattice constant. The curve fitting is obtained by a polynomial function. The equilibrium lattice constant was found to be 10.05 Å which agrees with results reported earlier [18,74].

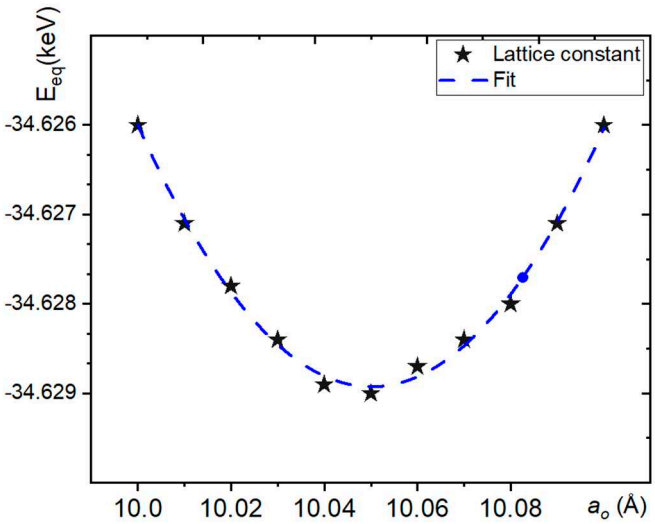

Figure 3. Relationship between system energy as function of lattice constants in $Yb_2Ti_2O_7$.

3.2. Threshold Displacement Energy (E_d)

The incident energy of primary knock-on atom (E_{PKA}) exceeds to overcome the constraints of the entire force field and leave a vacancy. This minimum energy (E_{min}) required to displace an atom from its lattice site is known as threshold displacement energy (E_d) [48]. The theoretical calculations displayed that off-site threshold energy depends on crystallographic direction, temperature, orientation of incident PKA, energy, and type of incident particles.

We have computed threshold energy of $Yb_2Ti_2O_7$ initially by selecting Yb, Ti with O atoms as incident PKA along [100], [110] and [111] axes. The E_d is displayed along the orientation in Figure 4. It can be seen that $E_{d\,(Yb)} >> E_{d\,(Ti)} > E_{d\,(O)}$. We have seen that E_d is anisotropic. Our finding are in agreement with other studies [92,93].

Preprints (www.preprints.org) | NOT PEER-REVIEWED | Posted: 18 August 2023 doi:10.20944/preprints202308.1329.v1

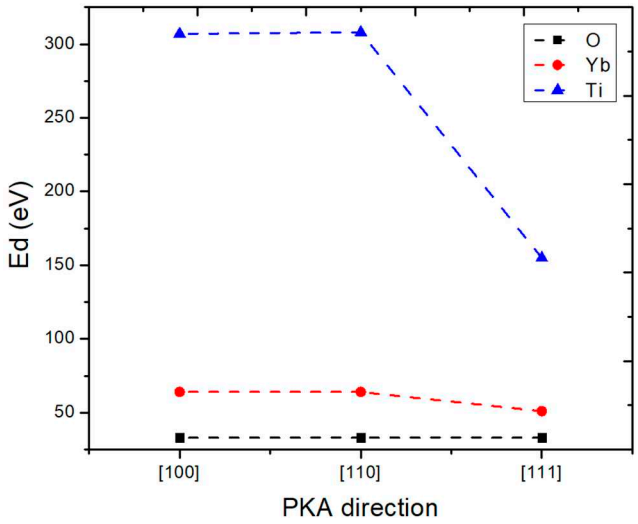

Figure 4. E_d as a function of incident PKA along with bombardment directions.

The calculation of the threshold energy (E_d) of high entropy pyrochlore $YbYTiZrO_7$ formed by doping Y element at A site and Zr element at B site. The atomic number ratio for simulated pyrochlore with substitution set as Yb:Y:Ti:Zr is 1:1:1:1. Later A-site is doped with three elements as Y, Eu, and Gd while B- site is doped with total of four elements in equal atomic proportion of seven constituent elements, i.e. Yb: Y: Gd: Eu: Ti: Zr as 1: 1: 1: 1 :1 : 2: 2 result in formation of $Yb_{0.5}Y_{0.5}Eu_{0.5}Gd_{0.5}TiZrO_7$. Table 4 compares the average E_d of two simulated models with incident PKA's directions. It is established that $E_d(Yb_{0.5}Y_{0.5}Eu_{0.5}Gd_{0.5}TiZrO_7) > E_d(Yb_2Ti_2O_7)$. This establishes that HEPy are less prone to defects [92].

Table 4. E_d as a function of different incident PKA's.

Types of PKA	PKA direction	E_d (eV)	Types of PKA	PKA direction	E_d (eV)
	[100]	60		[100]	1182
Yb	[110]	60	Ti	[110]	1177
	[111]	66		[111]	625
	[100]	146		[100]	430
Y	[110]	146	Zr	[110]	431
	[111]	174		[111]	426
	[100]	93		[100]	1769
Gd	[110]	93	O	[110]	1521
	[111]	84		[111]	343
	[100]	85			
Eu	[110]	85			
	[111]	128			

3.3. Effect of Displacement Cascades on Energy and Direction of PKA

Irradiated materials are associated with displacement cascades. The displacement cascades are divided into different subcascade during bombardment of incident neutrons and ion implantation. The displacement cascades with different incident PKA's are repress ted in Figure 5.

Preprints (www.preprints.org) | NOT PEER-REVIEWED | Posted: 18 August 2023 doi:10.20944/preprints202308.1329.v1

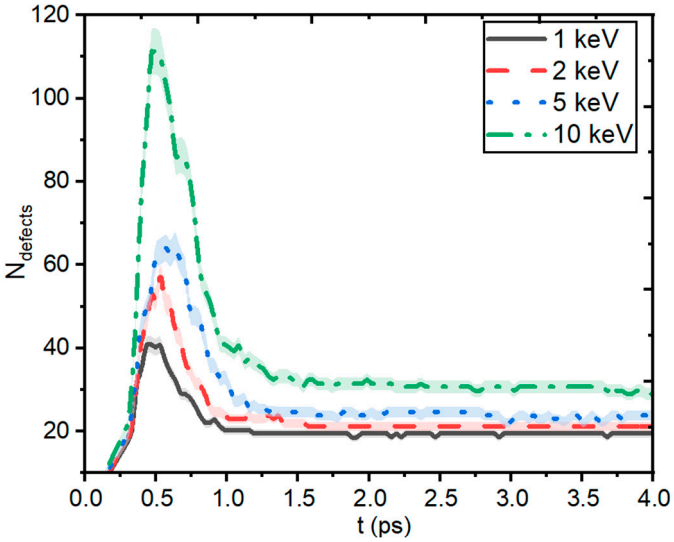

Figure 5. No of defects as a function of time under different energy PKA damage of $Yb_2Ti_2O_7$ bombarded with Yb ions of different energies.

As the energy of the initial PKA increases, the total number of defects of various atoms increases due to an increase in mean free path between atoms . Higher E_{PKA} produces larger area cascades which have higher possibility of reaching E_d [48]. The total number of defects will have a characteristic of rapid growth and then annihilate with time. This situation is generally referred to as defect recombination and permanent defect after radiation. In Figure 6, it can be noted that during the initial stage of the simulation cascade collision initiates a rapid accumulation of defects occurred in the pyrochlore lattice. The number of defects has reached a peak at 0.3ps and afterwards continuously reducing the size of cascade. The defects are stabilized at 0.9ps leaving permanent defects.

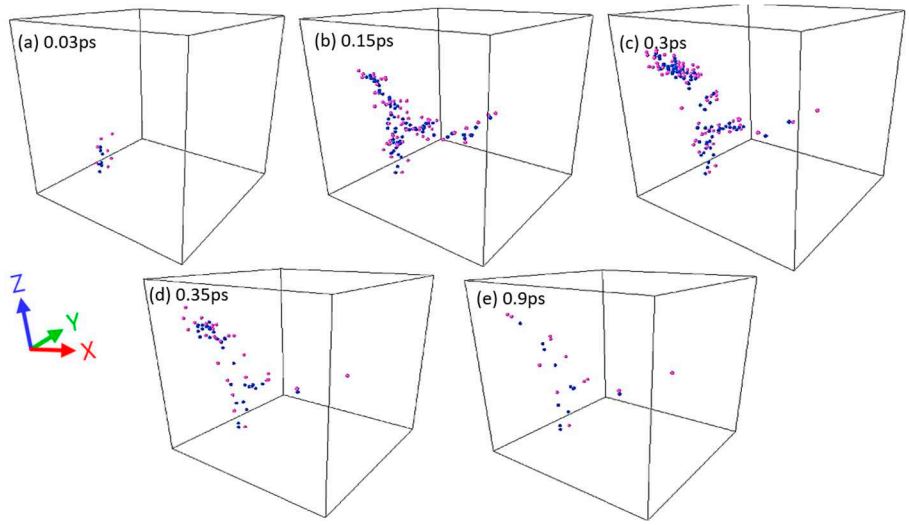

Figure 6. Displacement cascades in $Yb_2Ti_2O_7$ bombarded with 5keV Yb at different timesteps. Blue color are vacancies whereas purple is interstitials.

During the cascade simulations , incident PKA was located at the lower left corner and moved along the diagonal. The effect of incident direction is investigated by Yb incident with 5keV along X-axis inclined at 45° at different at an interval of 5° with 7° channeling angle along Z axis. The relation between incident angle as a function of time is expressed in Figure 7. It can be seen that the least number of defects smaller inclination angles have lower number of defects. This is due to the fact that higher inclination angles are associated with lower threshold energies of incident PKA's as well as successive overlapping cascades [94–96].

Preprints (www.preprints.org) | NOT PEER-REVIEWED | Posted: 18 August 2023 doi:10.20944/preprints202308.1329.v1

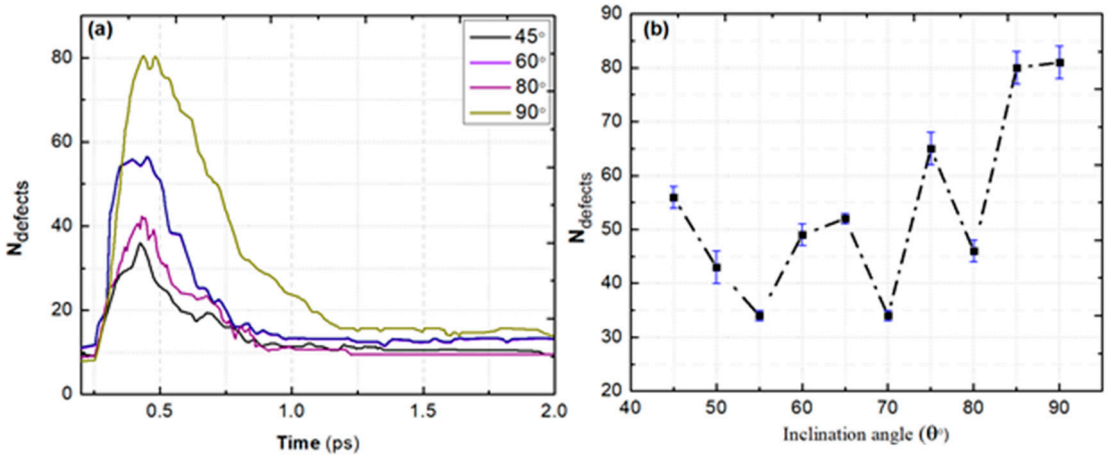

Figure 7. Number of surviving defects as function of **(a)** Time **(b)** inclination angle of incident 5keV Yb in $Yb_2Ti_2O_7$.

In order observe the effect of ions on inclination angle ,we compared the effect of defect evolution at lower and higher inclination angle by 5keV Yb atom. It is also known from Table 4 that Ti has higher values of E_d as compared to other constituents. The relation between number of defects as function of time are displayed in Figure 8 for different incident direction of PKA . It is clearly seen that Ti atoms and Yb atoms are almost the same in 55° (Figure 8 (a)) whereas Yb are double in Figure 8 (b). In both cases O has a higher number of defects than other constituents and higher angle has twice the number of defects .Therefore, it is more difficult to produce more defects in 55° inclination under the same energy of incident PKA.

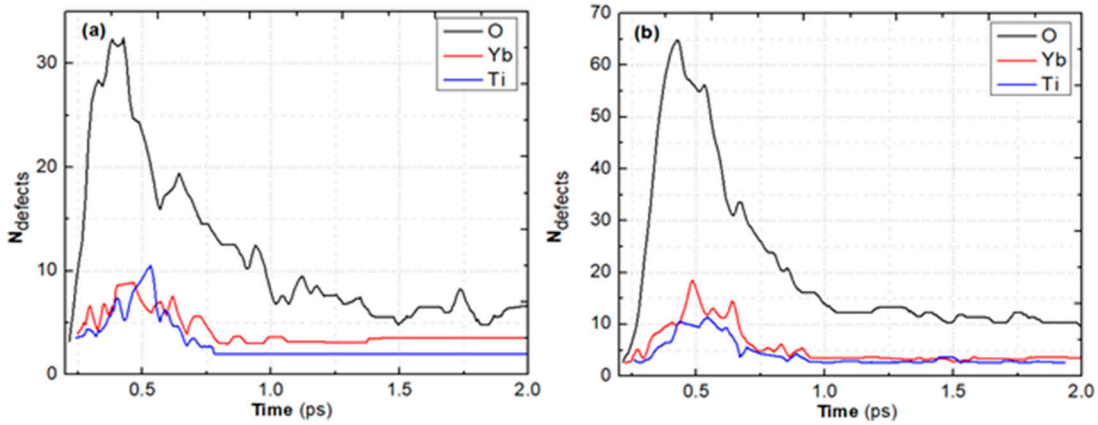

Figure 8. The number of defects of different types of atoms at an inclination of **(a)** 55°, **(b)** 85°.

3.4. Displacement Cascades in HEPy

This effect of displacement cascades on HEPy are studies by doping different elements on A and B sites of pyrochlore $Yb_2Ti_2O_7$ structure. We have selected Zr at B sites while A site is changed forming three kinds of HEPy i.e., Yb**Y**TiZrO_7 , Yb**Gd**TiZrO_7 , $Yb_{0.5}$**$Y_{0.5}$Eu$_{0.5}$Gd$_{0.5}$**TiZrO_7. The displacement cascades formed by Yb with 5keV and defects morphology in HEPy are compared with $Yb_2Ti_2O_7$. The comparison is based on the analysis and defect morphology.

Figure 9 displays the displacement cascades at its peak and after defect annihilation with Yb incident PKA of 5keV. The defect forms of $Yb_2Ti_2O_7$ and other three high-entropy pyrochlores are compared. The subscript for each displays the peak defects N_{max} and after annihilation. It is noted that the area of displacement cascades is larger for $Yb_2Ti_2O_7$ whereas number of defects formed by displacement cascades in HEPy are higher than pyrochlore whereas $Yb_{0.5}Y_{0.5}Eu_{0.5}Gd_{0.5}TiZrO_7$ has lower number of surviving defects . For all the models the direction of PKA coincides with the defects cluster direction. We have reasonable to believe that high-entropy pyrochlore has a better radiation resistance compared with $Yb_2Ti_2O_7$. It is also seen from the displacement cascade snapshots that

Preprints (www.preprints.org) | NOT PEER-REVIEWED | Posted: 18 August 2023 doi:10.20944/preprints202308.1329.v1

characteristic of limiting the circumferential development of defects and reducing the damage volume in HEPy.

Higher energies incident PKA are reported to have higher number of surviving defects [17,97,98]. The number of defects as function of time are compared for HEPy and pyrochlore are plotted in Figure 10. It can be seen from Figure 10 that the number of defects corresponding to YGdEu doped HEPy are lesser in all cases. The surviving defects in undoped pyrochlore are relatively larger than doped. The defect growth rate and defect disappearance rate of and the defect number annihilation is the faster in HEPy specially $Yb_{0.5}Y_{0.5}Eu_{0.5}Gd_{0.5}TiZrO_7$. It is preliminarily due to the fact that HEPy provides a large number of available atomic configurations, which can accommodate point defects and compensate for local structural changes induced by radiation. This configurational flexibility enhances the material's ability to self-heal and recover from radiation damage, further contributing to its lower radiation damage radius. This also establishes that HEPy shows a promising characteristic for radiation tolerance,. Thus, MD results in this study can be used to optimize the radiation resistant nature of HEPy by testing other models with orientation and other constituent elements in the composition.

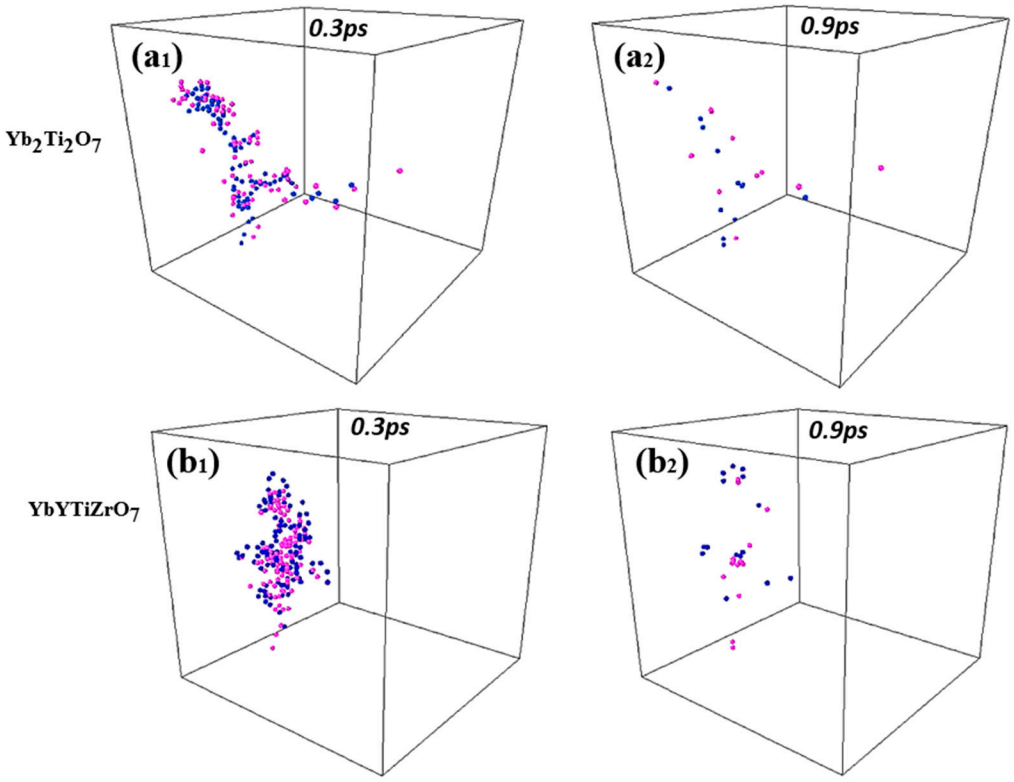

Preprints (www.preprints.org) | NOT PEER-REVIEWED | Posted: 18 August 2023 doi:10.20944/preprints202308.1329.v1

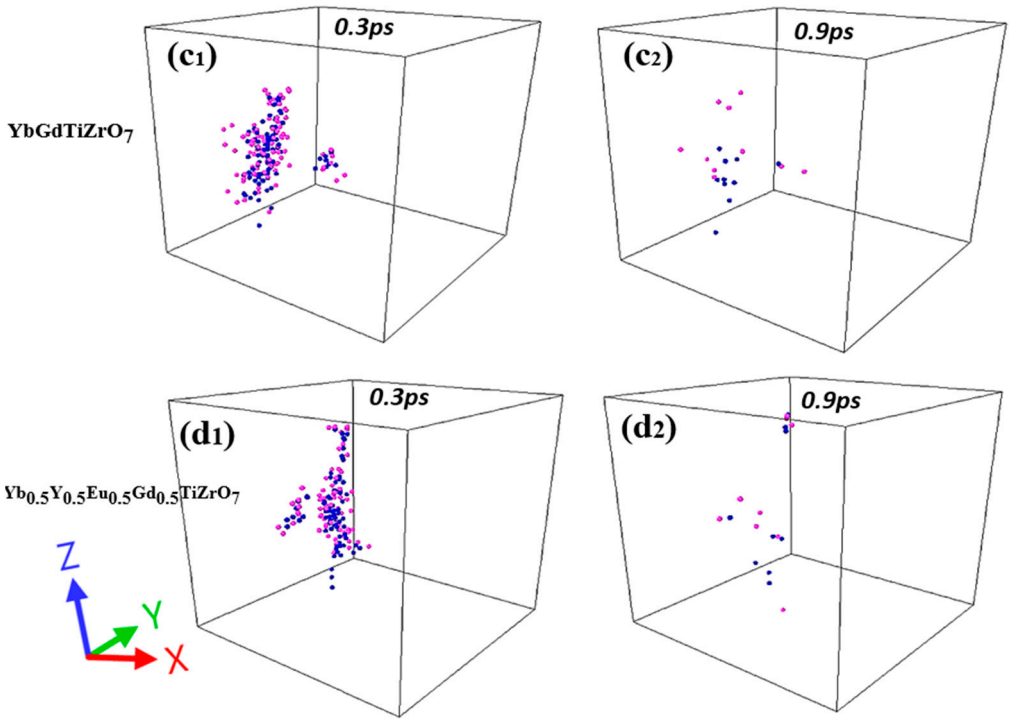

Figure 9. Displacement cascades in $Yb_2Ti_2O_7$ $YbYTiZrO_7$, $YbGdTiZrO_7$, $Yb_{0.5}Y_{0.5}Eu_{0.5}Gd_{0.5}TiZrO_7$.at timesteps 0.3ps and 0.9ps.

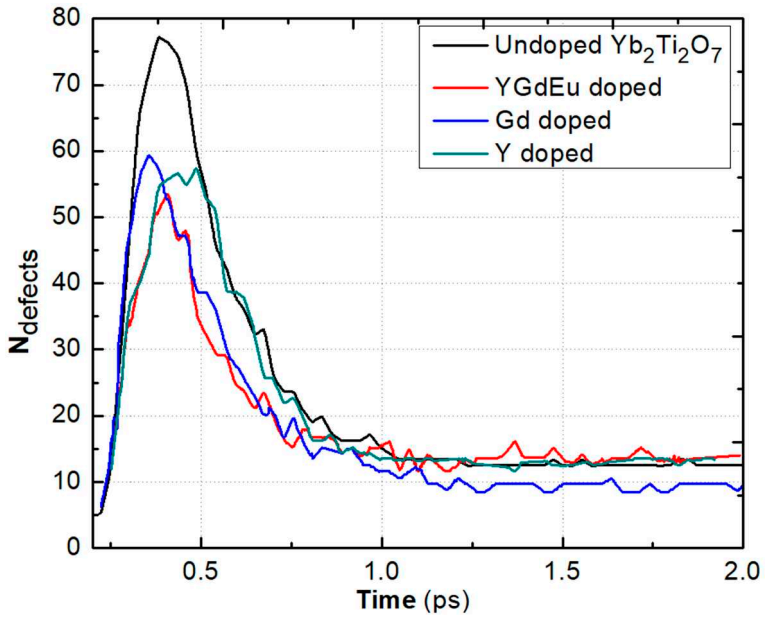

Figure 10. Defect evolution as function time in undoped $Yb_2Ti_2O_7$ and HEPy doped with Y ,Gd and YGdEu at the A sites.

4. Conclusion

Molecular dynamics simulations were performed to study the effect of displacement cascades in ytterbium titanate oxide ($Yb_2Ti_2O_7$) and high entropy alloys. The calculations for equilibrium lattice constant pyrochlore oxides. The displacement cascades in $Yb_2Ti_2O_7$ with Yb, Ti, O of 1 keV, 2keV, 5 keV, 10keV along [100], [110], [111] were used to determine the threshold energy (E_d) on the radiation damage response of pyrochlore. The effect of displacement cascades on the formation of high-entropy pyrochlore $YbYTiZrO_7$, $YbGdTiZrO_7$, $Yb_{0.5}Y_{0.5}Eu_{0.5}Gd_{0.5}TiZrO_7$ and $Yb_2Ti_2O_7$ was compared to analyze the radiation stability. The displacement cascades of different incident PKA display that number of defects are proportional to the incident energy . Higher incident angles have a lower number of defects. The defects morphology of HEPy was compared with $Yb_2Ti_2O_7$.

Author Contributions: Conceptualization QY(Qingyu Wang) MMA (M Mustafa Azeem.) and Y.Y.; methodology and software and validation .; supervision and project administration. All authors have read and agreed to the published version of the manuscript.

Funding: This research has no funding.

Data Availability Statement: data is contained within the article.

Acknowledgments: N/A.

Conflicts of Interest: The authors declare no conflict of interest.

References

[1] B. Raj, M. Vijayalakshmi, P.R. Vasudeva Rao, K.B.S. Rao, Challenges in materials research for sustainable nuclear energy, MRS Bull. 33 (2008) 327–337.

[2] P.W. Beck, NUCLEAR ENERGY IN THE TWENTY CENTURY: Examination of a Contentious Subject, Annu. Rev. Energy Environ. 24 (1999) 113–37.

[3] N. Mahmood, Danish, Z. Wang, B. Zhang, The role of nuclear energy in the correction of environmental pollution: Evidence from Pakistan, Nucl. Eng. Technol. 52 (2020) 1327–1333. https://doi.org/10.1016/j.net.2019.11.027.

[4] T. Abram, S. Ion, Generation-IV nuclear power: A review of the state of the science, Energy Policy. 36 (2008) 4323–4330. https://doi.org/10.1016/j.enpol.2008.09.059.

[5] K. Dungan, R.W.H. Gregg, K. Morris, F.R. Livens, G. Butler, Assessment of the disposability of radioactive waste inventories for a range of nuclear fuel cycles: Inventory and evolution over time, Energy. 221 (2021) 119826. https://doi.org/10.1016/j.energy.2021.119826.

[6] J. Amiard, Nuclear Waste Disposal Methods, Manag. Radioact. Waste. (2021) 23–66. https://doi.org/10.1002/9781119866480.ch2.

[7] L. Kong, I. Karatchevtseva, Y. Zhang, T. Wei, The incorporation of Nd or Ce in CaZrTi2O7 zirconolite: Ceramic versus glass-ceramic, J. Nucl. Mater. 543 (2021) 152583. https://doi.org/10.1016/j.jnucmat.2020.152583.

[8] Z. Liu, K. Liu, X. Zheng, Y. Wang, X. Sun, P. Xue, C. Li, M. Du, Formulation of Poly(ionic liquids)@COF Nanotrap for Efficient Perrhenate Sequestration from Alkaline Nuclear Waste, Chem. Mater. 34 (2022) 5452–5456. https://doi.org/10.1021/acs.chemmater.2c00377.

[9] X. Guo, S. Gin, G.S. Frankel, Review of corrosion interactions between different materials relevant to disposal of high-level nuclear waste, Npj Mater. Degrad. 4 (2020). https://doi.org/10.1038/s41529-020-00140-7.

[10] G.S. Frankel, J.D. Vienna, J. Lian, X. Guo, S. Gin, S.H. Kim, J. Du, J. V Ryan, J. Wang, W. Windl, C.D. Taylor, J.R. Scully, Recent Advances in Corrosion Science Applicable To Disposal of High-Level Nuclear Waste, Chem. Rev. 121 (2021) 12327–12383. https://doi.org/10.1021/acs.chemrev.0c00990.

[11] and H.F.S. Xu Huifang, Yifeng Wang, Pihong Zhao, William L. Bourcier, Richard Van Konynenburg, Investigation of Pyrochlore-Based U-Bearing Ceramic Nuclear Waste : Uranium Leaching Test and TEM Observation, Environ. Sci. Technol. 38 (2004) 1480–1486.

[12] M. Dholakia, S. Chandra, S.M. Jaya, Comparative study of radiation damage in Gd2Zr2O7 and Y2Ti2O7 crystal: A molecular dynamics investigation, AIP Conf. Proc. 2265 (2020) 30373. https://doi.org/10.1063/5.0017632.

[13] Y. Zhang, Ceramic Materials for Nuclear Energy Applications, JOM. 71 (2019) 4806–4807. https://doi.org/10.1007/s11837-019-03854-5.

[14] J. Marra, Advanced ceramic materials for next-generation nuclear applications, IOP Conf. Ser. Mater. Sci. Eng. 18 (2011) 16001. https://doi.org/10.1088/1757-899X/18/16/162001.

[15] W.H. Lee, J.H. Cheong, Potential radiological hazard and options to cope with consequences from recycling of activated metal waste disposed of at a near-surface disposal facility, Ann. Nucl. Energy. 152 (2021) 107993. https://doi.org/10.1016/j.anucene.2020.107993.

[16] M.L. Hand, M.C. Stennett, N.C. Hyatt, Rapid low temperature synthesis of a titanate pyrochlore by molten salt mediated reaction, J. Eur. Ceram. Soc. 32 (2012) 3211–3219. https://doi.org/10.1016/j.jeurceramsoc.2012.04.046.

[17] M. Dholakia, S. Chandra, Structural stability of titanate pyrochlores undergoing radiation damage, Comput. Mater. Sci. 201 (2022) 110889. https://doi.org/10.1016/j.commatsci.2021.110889.

[18] L. Minervini, R.W. Grimes, K.E. Sickafus, Disorder in pyrochlore oxides, J. Am. Ceram. Soc. 83 (2000) 1873–1878. https://doi.org/10.1111/j.1151-2916.2000.tb01484.x.
[19] L. Minervini, R.W. Grimes, K.E. Sickafus, Disorder in pyrochlore oxides, J. Am. Ceram. Soc. 83 (2000) 1873–1878. https://doi.org/10.1111/j.1151-2916.2000.tb01484.x.
[20] Y. Zhang, Machine learning the lattice constant of cubic pyrochlore compounds, Int. J. Appl. Ceram. Technol. 18 (2021) 661–676. https://doi.org/10.1111/ijac.13709.
[21] B.J. Kennedy, B.A. Hunter, C.J. Howard, Structural and Bonding Trends in Tin Pyrochlore Oxides, J. Solid State Chem. 130 (1997) 58–65. https://doi.org/10.1006/jssc.1997.7277.
[22] H. Sakai, K. Yoshimura, H. Ohno, H. Kato, S. Kambe, R.E. Walstedt, T.D. Matsuda, Y. Haga, Y. Onuki, Superconductivity in a pyrochlore oxide, Cd2Re2O7, J. Phys. Condens. Matter. 13 (2001). https://doi.org/10.1088/0953-8984/13/33/105.
[23] L. Dong, Y. Li, R. Devanathan, W. Setyawan, F. Gao, Low energy ion-solid interactions and chemistry effects in a series of pyrochlores, J. Am. Ceram. Soc. 100 (2017) 3132–3144. https://doi.org/10.1111/jace.14836.
[24] A. Chartier, C. Meis, J.P. Crocombette, L.R. Corrales, W.J. Weber, Atomistic modeling of displacement cascades in (formula presented) pyrochlore, Phys. Rev. B - Condens. Matter Mater. Phys. 67 (2003) 1–13. https://doi.org/10.1103/PhysRevB.67.174102.
[25] K.R. Whittle, M.G. Blackford, R.D. Aughterson, G.R. Lumpkin, N.J. Zaluzec, Ion irradiation of novel yttrium / ytterbium-based pyrochlores : The effect of disorder, Acta Mater. 59 (2011) 7530–7537. https://doi.org/10.1016/j.actamat.2011.09.021.
[26] A. Archer, H.R. Foxhall, N.L. Allan, J.R.W. Shearer, D.S.D. Gunn, J.H. Harding, I.T. Todorov, K.P. Travis, J.A. Purton, Multiple cascade radiation damage simulations of pyrochlore, Mol. Simul. 47 (2021) 273–283. https://doi.org/10.1080/08927022.2020.1805449.
[27] T. Subramani, A. Voskanyan, K. Jayanthi, M. Abramchuk, A. Navrotsky, A Comparison of Order-Disorder in Several Families of Cubic Oxides, Front. Chem. 9 (2021) 1–21. https://doi.org/10.3389/fchem.2021.719169.
[28] A. Annamareddy, J. Eapen, J. Eapen, Decoding ionic conductivity and reordering in cation-disordered pyrochlores Subject Areas : Author for correspondence :, Philos. Trans. A. 379 (2021).
[29] Z. Teng, Y. Tan, H. Zhang, High-entropy pyrochlore a2b2o7 with both heavy and light rare-earth elements at the a site, Materials (Basel). 15 (2022) 1–8. https://doi.org/10.3390/ma15010129.
[30] H. Xiang, Y. Xing, F. zhi Dai, H. Wang, L. Su, L. Miao, G. Zhang, Y. Wang, X. Qi, L. Yao, H. Wang, B. Zhao, J. Li, Y. Zhou, High-entropy ceramics: Present status, challenges, and a look forward, 2021. https://doi.org/10.1007/s40145-021-0477-y.
[31] M. Widom, Modeling the structure and thermodynamics of high-entropy alloys, J. Mater. Res. 33 (2018).
[32] Q. Zhi, X. Tan, Z. Liu, Y. Liu, Q. Zhang, Y. Chen, M. Li, Effect of Zr content on microstructure and mechanical properties of lightweight Al2NbTi3V2Zrx high entropy alloy, Micron. 144 (2021) 103031. https://doi.org/10.1016/j.micron.2021.103031.
[33] G. Ji, Z. Zhou, F. Meng, X. Yang, R. Sheng, J. Qiao, P.K. Liaw, M. Li, L. Jiang, S. Chen, Y. Tong, Effect of Zr addition on the local structure and mechanical properties of Ti–Ta–Nb–Zr refractory high-entropy alloys, J. Mater. Res. Technol. 19 (2022) 4428–4438. https://doi.org/10.1016/j.jmrt.2022.06.160.
[34] L.. Brixner, Preparation and Properties of the Ln2Ti20 -Type Rare Earth Titanates, Inorg. Chem. 3 (1964) 1065–1067. https://doi.org/10.1021/ic50017a049.
[35] Z. Wang, G. Zhou, D. Jiang, S. Wang, Recent development of A2B2O7 system transparent ceramics, J. Adv. Ceram. 7 (2018) 289–306. https://doi.org/10.1007/s40145-018-0287-z.
[36] M.M. Azeem, Q. Wang, Y. Zhang, S. Liu, M. Zubair, Effect of Grain Boundary on Diffusion of P in Alpha-Fe: A Molecular Dynamics Study, Front. Phys. 7 (2019) 1–7. https://doi.org/10.3389/fphy.2019.00097.
[37] M.M. Azeem, Z. Li, Q. Wang, A. Hussian, Molecular Dynamics Simulation Study on the Possible Factors Affecting Stability of ODS Steel, in: IOP Conf. Ser. Mater. Sci. Eng., 2018: p. 012003. https://doi.org/10.1088/1757-899X/389/1/012003.
[38] M. Mustafa Azeem, K. Abd El Gawad, M. Zubair, S.A. Ibrahim, M. Ado, G. Mehdi, Radiation damage effects in oxide dispersion strengthened steel alloys, in: Int. Conf. Nucl. Eng. Proceedings, ICONE, 2019. https://doi.org/10.1299/jsmeicone.2019.27.2086.
[39] M. Mustafa Azeem, Z. Li, Q. Wang, M. Zubair, Molecular dynamics studies and irradiation effects in ODSS alloys, Int. J. Nucl. Energy Sci. Technol. 12 (2018) 381–399. https://doi.org/10.1504/IJNEST.2018.097200.
[40] M.M. Azeem, Q. Wang, Z. Li, Y. Zhang, Dislocation-oxide interaction in Y2O3 embedded Fe: A molecular

dynamics simulation study, Nucl. Eng. Technol. 52 (2020) 337–343. https://doi.org/10.1016/j.net.2019.07.011.
[41] M.M. Azeem, Z. Li, Q. Wang, Q.M.N. Amjad, M. Zubair, O.M.H. Ahmed, Classical molecular dynamics study for defect sink behavior in oxide dispersed strengthened alloys, in: Proc. 2018 15th Int. Bhurban Conf. Appl. Sci. Technol. IBCAST 2018, 2018: pp. 12–15. https://doi.org/10.1109/IBCAST.2018.8312177.
[42] A.M. Mustafa, Z. Li, L. Shao, Molecular Dynamics Simulations of Damage Cascades Creation in Oxide-Particle-Embedded Fe., in: 25th Int. Conf. Nucl. Eng., 2017: pp. 1–5. https://doi.org/10.1115/ICONE25-67356.
[43] M.M. Azeem, Q. Wang, M. Zubair, Atomistic simulations of nanoindentation response of irradiation defects in iron, Sains Malaysiana. 48 (2019) 2029–2039. https://doi.org/10.17576/jsm-2019-4809-24.
[44] M.M. Azeem, D. Yun, M. Zubair, Atomic insights on interaction mechanism of dislocation with void/impurity/ precipitates in bcc iron, Int. Conf. Nucl. Eng. Proceedings, ICONE. 2 (2021) 1–7. https://doi.org/10.1115/ICONE28-65197.
[45] G. Vinothkumar, S. Rengaraj, P. Arunkumar, S.W. Cha, K.S. Babu, and La 3 +) - Doped Cerium Oxide Nanoparticles for Enhanced Multienzyme-Mimetic and Hydroxyl Radical Scavenging Activity, (2019). https://doi.org/10.1021/acs.jpcc.8b10108.
[46] A. Garbout, S. Bouattour, M. Ellouze, A.W. Kolsi, Synthesis, FT-IR and X-ray diffraction investigations of gadolinium-substituted pyrochlore oxide Gd1.82Cs0.18Ti2O6.82 via a sol-gel process, J. Alloys Compd. 425 (2006) 88–95. https://doi.org/10.1016/j.jallcom.2006.01.084.
[47] D.S.D. Gunn, N.L. Allan, H. Foxhall, J.H. Harding, J.A. Purton, W. Smith, M.J. Stein, I.T. Todorov, K.P. Travis, Novel potentials for modelling defect formation and oxygen vacancy migration in Gd 2Ti 2O 7 and Gd 2Zr 2O 7 pyrochlores, J. Mater. Chem. 22 (2012) 4675–4680. https://doi.org/10.1039/c2jm15264a.
[48] R. Devanathan, W.J. Weber, Insights into the radiation response of pyrochlores from calculations of threshold displacement events, J. Appl. Phys. 98 (2005). https://doi.org/10.1063/1.2120889.
[49] X.J. Wang, H.Y. Xiao, X.T. Zu, Y. Zhang, W.J. Weber, Ab initio molecular dynamics simulations of ion–solid interactions in Gd 2 Zr 2 O 7 and Gd 2 Ti 2 O 7, J. Mater. Chem. C. 1 (2013) 1665–1673.
[50] E.R. Aluri, A.P. Grosvenor, An X-ray absorption spectroscopic study of the effect of bond covalency on the electronic structure of Gd2Ti2-xSnxO 7, Phys. Chem. Chem. Phys. 15 (2013) 10477–10486. https://doi.org/10.1039/c3cp51250a.
[51] S. Zheng, S. Wang, First-principles design of refractory high entropy alloy VMoNbTaW, Entropy. 20 (2018). https://doi.org/10.3390/e20120965.
[52] K. Lipkina, A. Savchenko, M. Skupov, A. Glushenkov, A. Vatulin, O. Uferov, Y. Ivanov, G. Kulakov, S. Ershov, S. Maranchak, A. Kozlov, E. Maynikov, K. Konova, Metallic inert matrix fuel concept for minor actinides incineration to achieve ultra-high burn-up, J. Nucl. Mater. 452 (2014) 378–381. https://doi.org/10.1016/j.jnucmat.2014.04.030.
[53] M.K. Anupama, B. Rudraswamy, Effect of Gd3+- Cr3+ ion substitution on the structural, electrical and magnetic properties of Ni - Zn ferrite nanoparticles, in: IOP Conf. Ser. Mater. Sci. Eng., 2016. https://doi.org/10.1088/1757-899X/149/1/012194.
[54] L. Chen, X. Su, Y. Li, First-Principles Study on Cation-Antisite Defects of Stannate and Titanate Pyrochlores, OALib. 01 (2014) 1–8. https://doi.org/10.4236/oalib.1100516.
[55] Y. Yang, W. Wang, G.-. Y. Gan, X.-. F. Shi, B.-. Y. Tang, Structural, mechanical and electronic properties of (TaNbHfTiZr)C high entropy carbide under pressure: ab initio investigation, Phys. B. 550 (2018).
[56] W. Akhtar, M.M. Azeem, M.B. Khan, M. Science, Atomistic Insights into the Irradiation Effects in Molybdenum, Int. J. Eng. Work. 9 (2022) 187–192.
[57] A. Ullah, Q. Wang, Y. Song, M.M. Azeem, M. Ado, M. Sohail, Continuous Stiffness Measurements and Nanoindentation Studies of bcc Mo: An Atomistic Approach, Trans. Indian Inst. Met. 75 (2022) 1555–1561. https://doi.org/10.1007/s12666-022-02524-6.
[58] S.A. Ibrahim, Q. Wang, Y. Zhang, M. Ado, G.D. Chung, M.M. Azeem, Molecular dynamics simulation of strengthening dependence on precipitate Cr composition in Fe-15at.%Cr alloy, Micron. 131 (2020) 102823. https://doi.org/10.1016/j.micron.2020.102823.
[59] A. Ullah, W. Qingyu, M. Ado, M.M. Azeem, A. Shah, Effect of Concentration of Mo on the Mechanical behavior of γ UMo: an Atomistic Study, Pet. Chem. Ind. Int. 4 (2021) 67–71. https://doi.org/10.33140/pcii.04.03.05.
[60] M.M. Azeem, D. Yun, M. Zubair, Atomic Insights on Interaction Mechanism of Dislocation With Void/Impurity/Precipitates in BCC Iron, in: Proc. 2021 28th Int. Conf. Nucl. Eng., 2021. https://doi.org/10.1115/ICONE28-65197.

[61] A.K.D. Willie, H. Zhao, M. Mustafa Azeem, T. Svetlana, Analysis of Burnup effects and Its Integrity Assessment in the Interim of Irradiation with Molecular Dynamics, MRS Adv. 5 (2020) 1799–1810. https://doi.org/10.1557/adv.2020.19.

[62] S.A. Ibrahim, Q. Wang, M. Ado, M. Mustafa Azeem, Z. Abbati, Irradiation effects of Fe-Cr alloys, in: Int. Conf. Nucl. Eng. Proceedings, ICONE, 2019. https://doi.org/10.1299/jsmeicone.2019.27.1201.

[63] G. Mehdi, N. Ali, S. Hussain, A.A. Zaidi, A. Hussain Shah, M.M. Azeem, Design and fabrication of automatic single axis solar tracker for solar panel, in: 2019 2nd Int. Conf. Comput. Math. Eng. Technol. ICoMET 2019, 2019. https://doi.org/10.1109/ICOMET.2019.8673496.

[64] A.M.M. Eltayeb Yousif, Zhang Zhijian, Tian Zhao-fe, A Simulation of Small Break Loss of Coolant Accident (SB-LOCA) in AP1000 Nuclear Power Plant Using RELAP5-MV, 25th Int. Conf. Nucl. Eng. 5 (2017) 1–5. https://doi.org/10.1115/ICONE25-67469.

[65] O.M.H. Ahmed, F.I. Habbani, A.M. Mustafa, E.M.A. Mohamed, A.M. Salih, F. Seedig, Quality Assessment Statistic Evaluation of X-Ray Fluorescence via NIST and IAEA Standard Reference Materials, World J. Nucl. Sci. Technol. 07 (2017) 121–128. https://doi.org/10.4236/wjnst.2017.72010.

[66] M.M. Azeem, I. Jamil, M. Khan, Multiscale Modeling of Radiation Damage in Oxide Dispersed Strengthened Steel Alloys : A Perspective, Int. J. Eng. Work. 9 (2022) 193–200.

[67] M.M. Azeem, Z. Li, Q. Wang, A. Hussian, Molecular Dynamics Simulation Study on the Possible Factors Affecting Stability of ODS Steel, IOP Conf. Ser. Mater. Sci. Eng. 389 (2018) 12003. https://doi.org/10.1088/1757-899X/389/1/012003.

[68] M. Zubair, A. Wakeel, M.M. Azeem, A. Tabbassum, Computational analysis of high carbon steel for optimal design, Proc. 18th Int. Bhurban Conf. Appl. Sci. Technol. IBCAST 2021. (2021) 10–14. https://doi.org/10.1109/IBCAST51254.2021.9393173.

[69] M. V. Talanov, V.M. Talanov, Structural Diversity of Ordered Pyrochlores, Chem. Mater. 33 (2021) 2706–2725. https://doi.org/10.1021/acs.chemmater.0c04864.

[70] T. Connor, O. Cheong, T. Bornhake, A.C. Shad, R. Tesch, M. Sun, Z. He, A. Bukayemsky, V.L. Vinograd, Pyrochlore Compounds From Atomistic Simulations, Front. Chem. 9 (2021) 1–14. https://doi.org/10.3389/fchem.2021.733321.

[71] R.C. Ewing, W.J. Weber, J. Lian, Nuclear waste disposal-pyrochlore (A 2B 2O 7): Nuclear waste form for the immobilization of plutonium and “minor” actinides, J. Appl. Phys. 95 (2004) 5949–5971. https://doi.org/10.1063/1.1707213.

[72] K. Momma, F. Izumi, VESTA 3 for three-dimensional visualization of crystal, volumetric and morphology data, J. Appl. Crystallogr. 44 (2011) 1272–1276. https://doi.org/10.1107/S0021889811038970.

[73] K.B. Wiberg, A Scheme for Strain Energy Minimization. Application to the Cycloalkanes, J. Am. Chem. Soc. 87 (1965) 1070–1078. https://doi.org/10.1021/ja01083a024.

[74] V. Kocevski, G. Pilania, B.P. Uberuaga, Modeling Disorder in Pyrochlores and Other Anion-Deficient Fluorite Structural Derivative Oxides, Front. Chem. 9 (2021) 1–10. https://doi.org/10.3389/fchem.2021.712543.

[75] B.C. Chakoumakos, Systematics of the pyrochlore structure type, ideal A2B2X6Y, J. Solid State Chem. 53 (1984) 120–129. https://doi.org/10.1016/0022-4596(84)90234-2.

[76] K.E. Sickafus, L. Minervini, R.W. Grimes, J.A. Valdez, M. Ishimaru, F. Li, K.J. McClellan, T. Hartmann, Radiation tolerance of complex oxides, Science (80-.). 289 (2000) 748–751. https://doi.org/10.1126/science.289.5480.748.

[77] S. Plimpton, B. Hendrickson, A New Parallel Method for Molecular Dynamics Simulation of Macromolecular Systems, J. Comput. Chem. 17 (1996) 326–337. https://doi.org/10.1002/(SICI)1096-987X(199602)17:3<326::AID-JCC7>3.0.CO;2-X.

[78] A. Stukowski, Visualization and analysis of atomistic simulation data with OVITO the Open Visualization Tool, Model. Simul. Mater. Sci. Eng. 18 (2010) 015012. https://doi.org/10.1088/0965-0393/18/1/015012.

[79] M. Dholakia, S. Chandra, S.M. Jaya, A comparative study of topology and local disorder in Y2O3, Y2TiO5, and Y2Ti2O7 crystals Manan, J. Alloys Compd. 739 (2018) 1037–1047. https://doi.org/10.1016/j.jallcom.2017.12.244.

[80] L. Minervini, R.W. Grimes, Y. Tabira, R.L. Withers, K.E. Sickafus, The oxygen positional parameter in pyrochlores and its dependence on disorder, Philos. Mag. A Phys. Condens. Matter, Struct. Defects Mech. Prop. 82 (2002) 123–135. https://doi.org/10.1080/01418610208240001.

[81] G. Balducci, J. Kašpar, P. Fornasiero, M. Graziani, M.S. Islam, Surface and reduction energetics of the CeO2-

ZrO2 catalysts, J. Phys. Chem. B. 102 (1998) 557–561. https://doi.org/10.1021/jp972400n.

[82] B.A. Luty, M.E. Davis, I.G. Tironi, W.F. Van Gunsteren, A comparison of particle-particle, particle-mesh and ewald methods for calculating electrostatic interactions in periodic molecular systems, Mol. Simul. 14 (1994) 11–20. https://doi.org/10.1080/08927029408022004.

[83] J.F. Ziegler, J.P. Biersack, The Stopping and Range of Ions in Matter BT - Treatise on Heavy-Ion Science: Volume 6: Astrophysics, Chemistry, and Condensed Matter, in: D.A. Bromley (Ed.), Springer US, Boston, MA, 1985: pp. 93–129. https://doi.org/10.1007/978-1-4615-8103-1_3.

[84] M.W.D. Cooper, M.J.D. Rushton, R.W. Grimes, A many-body potential approach to modelling the thermomechanical properties of actinide oxides, J. Phys. Condens. Matter. 26 (2014). https://doi.org/10.1088/0953-8984/26/10/105401.

[85] M. Ado, Q. Wang, S.A. Ibrahim, S.O. Adede, Effect of radiation and substitution of Ce4+ at Zr site in Y4Zr3O12 using collision cascades: a molecular dynamics simulation study, J. Nucl. Sci. Technol. 00 (2022) 1–10. https://doi.org/10.1080/00223131.2022.2122615.

[86] S. Plimpton, Fast parallel algorithms for short-range molecular dynamics, J. Comput. Phys. 117 (1995) 1–19. https://doi.org/10.1006/jcph.1995.1039.

[87] M. Duvail, P. Vitorge, R. Spezia, Building a polarizable pair interaction potential for lanthanoids (III) in liquid water : A molecular dynamics study of structure and dynamics of the whole series Building a polarizable pair interaction potential for lanthanoids „ III … in liquid water , (2009). https://doi.org/10.1063/1.3081143.

[88] R. Nakamoto, B. Xu, C. Xu, H. Xu, L. Bellaiche, Properties of rare-earth iron garnets from first principles, Phys. Rev. B. 95 (2017) 024434. https://doi.org/10.1103/PhysRevB.95.024434.

[89] W. Lee, S.Y. Chen, E. Tseng, A. Gloter, C.L. Chen, Study of defect structure in ferromagnetic nanocrystalline CeO2: Effect of ionic radius, J. Phys. Chem. C. 120 (2016) 14874–14882. https://doi.org/10.1021/acs.jpcc.6b02817.

[90] H. Yamamura, H. Nishino, K. Kakinuma, K.N. Þ, Crystal Phase and Electrical Conductivity in the Pyrochlore - Type, J. Ceram. Sociery Japan. 11 (2003) 902–906.

[91] M.A. Subramanian, G. Aravamudan, G. V. Subba Rao, Oxide pyrochlores - A review, Prog. Solid State Chem. 15 (1983) 55–143. https://doi.org/10.1016/0079-6786(83)90001-8.

[92] L. Dong, Y. Li, R. Devanathan, F. Gao, Molecular dynamics simulation of the structural, elastic, and thermal properties of pyrochlores, RSC Adv. 6 (2016) 41410–41419. https://doi.org/10.1039/c6ra04779c.

[93] L. Dong, W. Setyawan, Y. Li, R. Devanathan, F. Gao, Molecular dynamics simulation of low-energy recoil events in titanate pyrochlores, RSC Adv. 7 (2017) 35403–35410. https://doi.org/10.1039/c7ra04699e.

[94] A.E. Sand, K. Nordlund, S.L. Dudarev, Radiation damage production in massive cascades initiated by fusion neutrons in tungsten, J. Nucl. Mater. 455 (2014) 207–211. https://doi.org/10.1016/j.jnucmat.2014.06.007.

[95] N. Chen, D. Huang, E.R. Heller, D.A. Cardimona, F. Gao, Atomistic simulation of displacement damage and effective nonionizing energy loss in InAs, Phys. Rev. Mater. 5 (2021). https://doi.org/10.1103/PhysRevMaterials.5.033603.

[96] R. Devanathan, W.J. Weber, F. Gao, Atomic scale simulation of defect production in irradiated 3C-SiC, J. Appl. Phys. 90 (2001) 2303–2309. https://doi.org/10.1063/1.1389523.

[97] B.P. Mandal, K. Bhattacharyya, J.H. Zain, V. Sudarsan, S. Nigam, C. Nayak, A.K. Tyagi, Variation of structural disorder in Zr substituted Y2Sn2O7: Its impact on photocatalysis, J. Solid State Chem. 303 (2021) 122472. https://doi.org/10.1016/j.jssc.2021.122472.

[98] L. Cai, A.L. Arias, J.C. Nino, The tolerance factors of the pyrochlore crystal structure, J. Mater. Chem. 21 (2011) 3611–3618. https://doi.org/10.1039/c0jm03380d.